

# Measuring the scatter of the mass-richness relation in galaxy clusters in photometric imaging surveys by means of their correlation function

Julia Campa <sup>1,2,3</sup>

campa@fnal.gov

Brenna Flaugher<sup>1</sup>

and

Juan Estrada <sup>1</sup>

Received \_\_\_\_\_; accepted \_\_\_\_\_

---

<sup>1</sup>Center for Particle Astrophysics, Fermi National Accelerator Laboratory, Batavia, IL

<sup>2</sup>Centro de Investigaciones Energéticas, Medioambientales y Tecnológicas (CIEMAT),  
Madrid, Spain

<sup>3</sup>Universidad Autònoma de Barcelona (UAB), Bellaterra, Barcelona, Spain

## ABSTRACT

The knowledge of the scatter in the mass-observable relation is a key ingredient for a cosmological analysis based on galaxy clusters in a photometric survey. We demonstrate here how the linear bias measured in the correlation function for clusters can be used to determine the value of the scatter. The new method is tested in simulations of a 5,000  $deg^2$  optical survey up to  $z \sim 1$ , similar to the ongoing Dark Energy Survey. The results indicate that the scatter can be measured with a precision of 5% using this technique.

*Subject headings:* cosmology: observations-cosmology-galaxies: clusters: general-large-scale structure of universe

## 1. Introduction

The discovery of late time cosmic acceleration from observations of supernovae in 1998 is one of the most important development of modern cosmology (Riess et al. (1998), Perlmutter et al. (1999)). It raises fundamental questions about the expanding universe and our understanding of gravity. The cosmic acceleration could arise from the repulsive gravity of dark energy or it may be signal that General Relativity breaks down on cosmological scales and must be replaced (e.g., Copeland et al. (2006); Clifton et al. (2012)). Apart from distance measurements using type Ia supernovae, there are other methods such as weak gravitational lensing of matter distribution or galaxy cluster surveys to test these theories at recent epoch (e.g., Weinberg et al. (2013)).

Clusters of galaxies were first identified as over-dense regions in the projected number counts of galaxies (e.g., Abell (1958); Zwicky et al. (1968)). They are the most virialized systems known in the Universe and have a long history as cosmological probes.

The abundance of galaxy clusters as a function of mass can be used to constrain cosmological parameters (e.g., White et al. (1993); Rozo et al. (2010); Allen et al. (2011), Bocquet et al. (2015) ) and they are also a powerful tool for large scale studies (e.g., Bahcall (1998); Bahcall et al. (2003); Einasto (2001); Yang et al. (2005); Papovich (2008) and Willis et al. (2013)).

The quantity most tightly constrained by cluster abundance is a combination of the form  $\sigma_8 \Omega_m^q$ . However, the statistical power of large solid angle cluster surveys will allow us to break the degeneracy between  $\sigma_8$  and  $\Omega_m$ . The evolution of cluster abundance with redshift is highly sensitive to cosmology because the matter density,  $\Omega_m$  controls the rate at which structure grows. The evolution of the abundance will also allow us to constrain the equation of state,  $w$  (e.g., Eke et al. (1998); Haiman et al. (2001); Mohr (2005)) and to parametrize deviations from General Relativity (e.g., Cataneo et al. (2015)).

The number density of virialized dark matter halos as a function of redshift and halo mass can be accurately predicted from N-body simulations (e.g., Sheth & Tormen (1999); Jenkins et al. (2001); Reed et al. (2003); Warren et al. (2006); Lukić et al. (2007); Tinker et al. (2008); Crocce et al. (2010); Angulo et al. (2012); Watson et al. (2013)). Comparing these predictions to the evolution of the abundance of galaxy clusters in large-area surveys that extend to high redshift ( $z \geq 1$ ) can provide precise constraints on the cosmological parameters.

Massive galaxy clusters can be identified via optical (e.g., Soares-Santos et al. (2011) and Rykoff et al. (2014)), X-ray emission (e.g., Vikhlinin et al. (1998), Böhringer et al. (2000) and Pacaud et al. (2007)) and Sunyaev-Zeldovich effect (SZE) (e.g., Planck Collaboration et al. (2014) and Bleem et al. (2015)) observables. Their masses can be estimated in a number of different ways using these detections. However, these estimators are always indirect and inferred from observables correlated with mass. Since the number density for clusters is a strong function of mass, a well understood mass-observable relation is required to recover the cosmological information. Uncertainties in the mass-observable relation are the main challenge for cosmological studies with clusters, and could destroy most of the cosmological information in cluster counts if it is not well calibrated (e.g., Lima & Hu (2005)). The calibration task is to determine the mean relation and the dispersion of the mass-observable relation (called “scatter”) and to characterise deviations from lognormal form that are large enough to affect the predicted abundance (e.g., Shaw et al. (2010)).

There is a long history of cluster samples selected from optical and near infrared photometric surveys (e.g., Gladders & Yee (2000); Koester et al. (2007); Hao et al. (2010); Rykoff et al. (2014); Bleem et al. (2015)), and large scale optical surveys will soon be available from ongoing and future surveys such as the Dark Energy Survey (DES, Flaugher

(2005))<sup>1</sup>, Euclid (Laureijs et al. 2011) and the Large Synoptic Survey Telescope (LSST; LSST Dark Energy Science Collaboration (2012)). They are expected to generate galaxy catalogs to sufficient depth to reliably detect clusters at redshifts as high as  $z \sim 1$ .

In order to overcome the degeneracy between cosmological parameters and mass calibration parameters, self-calibration techniques have been developed (e.g., Schuecker et al. (2003), Majumdar & Mohr (2004), Lima & Hu (2005), Oguri & Takada (2011) and Andreon & Bergé (2012)). The relation is calibrated using a large cluster sample complemented with statistical properties of the cluster that are sensitive to mass. One parametrizes the mass-observable relation and then use standard likelihood methods to jointly fit for both cosmology and mass-observable parameters.

The uncertainty in the scatter for the mass-observable relation translates into a systematic uncertainty in the determination of cosmological parameters. This systematic effect has been studied for constraining dark energy parameters in a cluster counting experiment for an imaging survey with an area of 5000  $deg^2$ , similar to the ongoing Dark Energy Survey. Rozo et al. (2011) studied when a source of scatter is observationally relevant with the standard calibration with a fiducial cluster sample. Their conclusions are that if the accuracy to measure the scatter,  $\sigma_{true} - \sigma_{model}$ , is  $\geq 0.05$ , the recovered dark energy parameters will be significantly biased and the source of noise will be observationally relevant.

In this paper, we present a new method to constrain the scatter of the mass-observable relation for ongoing and future wide area photometric surveys. We show that the amplitude of the correlation function of clusters (i.e., Bahcall et al. (2003), Bahcall & Soneira (1983), Estrada et al. (2009)) provides information about the mass-observable relation (Majumdar

---

<sup>1</sup><http://www.darkenergysurvey.org>

& Mohr 2004), and can be used to constrain the scatter. This method is complementary to self-calibration and cross-calibration techniques in multiwavelength data from so called direct mass measurement (e.g., Rozo et al. (2009) and Saro et al. (2015)).

To ensure that the scatter and other systematics are under control, the DES collaboration has pursued the development of multiple cluster finder algorithms. Saro et al. (2015) study the mass-richness relation and the scatter for a small subset of SZE selected clusters of the South Pole Telescope (SPT; Bleem et al. (2015)) with optically selected clusters in the DES Science Verification Area (SVA). The new analysis technique proposed in this work can be implemented as a cross-check of this study in the DES data and other photometric surveys to reduce the uncertainty in cosmological parameters coming from an uncertainty in the scatter in the mass-richness relation.

The plan of this paper is the following. In Section 2 we describe the mass-richness relation that we are going to use in this work to add the galaxies to the dark matter halo in simulations. In Section 3, we introduce the theoretical model for the bias to compare with observations in optical surveys such as DES. We define the bias using the Halo Model of Galaxy Clustering. We require a Halo Occupation Distribution (HOD) where the mean number of galaxies is specified. In Section 4, previous to studying the bias in clusters, we study the accuracy of the halo mass function and bias in the light cone simulations. In Section 5, we describe our simulated cluster sample based on the dark matter halo simulations. In Section 6, we define our model for the bias when we make cuts in richness to compare with the measurements in simulations. In Section 7 we will show how measurements of the clustering of clusters can constrain the scatter of the scaling relation. We will make a forecast of the performance of the new analysis technique for DES. We end with a summary and conclusions in Section 8.

## 2. Mass-richness relation in galaxy clusters

The main observational challenges when using clusters to constrain cosmology are the cluster detection algorithm and the cluster mass estimation. The advent of multi-band data has led to a proliferation of optical cluster-finding algorithms. These algorithms use various techniques for measuring clustering in angular position plus color/redshift space, ranging from simple matched filters to Voronoi tessellations. These cluster finders estimate a richness that correlates with external mass proxies and then the mass-richness relation can be calibrated. Some examples of the matched filter algorithms that use the red-sequence are the maxBCC (Koester et al. 2007) and the more modern redMaPPer (Rykoff et al. 2014). The Voronoi Tessellation (VT; Soares-Santos et al. (2011)) algorithm uses photometric redshift to detect clusters in 2+1 dimensions.

Although the mass-richness relation is being calibrated using many cluster finder algorithms such as redMaPPer and the VT algorithms in the DES footprint (e.g., Saro et al. (2015)), we are going to use the form of the mean relation between the cluster mass and richness used in Rozo et al. (2009) to test our method in simulations. It is based on the results from the statistical weak lensing analysis in the maxBCG cluster catalog (Koester et al. 2007). This algorithm identifies clusters using two optical properties. First, the brightest cluster galaxy (BCG) typically lies near the center of the cluster galaxy light distribution. Second, the cores of rich clusters are dominated by red-sequence galaxies that occupy a narrow locus in color-magnitude space, the E/SO ridge line. MaxBCG uses a maximum-likelihood method to evaluate the probability that a given galaxy is a BCG near the center of a red-sequence galaxy density excess.

Every cluster is also assigned a richness measure  $N_{200}$ , which is the number of red sequence galaxies above a luminosity cut of  $0.4L_*$  and within a specified scaled aperture, centered on the Brightest Cluster Galaxy (BCG) of each cluster.

The separate statistical weak lensing measurement of Johnston et al. (2007), Mandelbaum et al. (2008), Mandelbaum et al. (2008), indicate that  $N_{200}$  is strongly correlated with cluster virial mass. These analyses are discussed in the Appendix of Rozo et al. (2009) and yield a relation between cluster mass and richness given by,

$$\frac{\langle M|N_{200} \rangle}{10^{14}} = \exp^{B_{M|N_{200}}} \left( \frac{N_{200}}{40} \right)^{\alpha_{M|N_{200}}} \quad (1)$$

where  $\alpha_{M|N} = 1.06 \pm 0.08(stat) \pm 0.23(sys)$  and  $B_{M|N} = 0.95 \pm 0.07(stat) \pm 0.10(sys)$  are the priors described in Rozo et al. (2009). We take them as the fiducial values of the mass-richness relation parameters.

### 3. A model for the galaxy cluster correlation function

In this section the clustering of clusters is predicted using the halo model of galaxy clustering (i.e. Cooray & Sheth (2002)). In order to compute clustering statistics, it is necessary to specify the number of galaxies per clusters using a Halo Occupation Distribution (HOD) and the spatial and velocity distributions of galaxies within halos (e.g., Neyman & Scott (1952); Berlind & Weinberg (2002); Baugh (2013); Pujol & Gaztañaga (2014)). One can then calculate the clustering of clusters from the combination of the HOD with the clustering of halos if we assume that the clustering of halos depends only of the halo mass. There are discussions about the dependency of the HOD on the cosmic environment in addition to the mass of the halo (e.g., Croft et al. (2012)), however we develop the formalism of the halo model keeping it as simple as possible.

From the assumption that all galaxies reside within dark matter halos it follows immediately that given a halo population and a HOD, we can calculate the correlation function of clusters. This is written as the sum of the one halo term and the two halo term. On large scales the two halo term dominates the correlation function and it can

be expressed in terms of the weighted value of the halo bias. Thus, the galaxy cluster correlation function simplifies to

$$\xi_{cc}(\bar{r}, z) = b^2(z)\xi_{mm}(\bar{r}, z) \quad (2)$$

where  $b(z)$  is the mean large scale bias of a particular galaxy population at redshift  $z$  that we assume is constant at large scales. The dark matter correlation function,  $\xi_{mm}$ , is obtained via Fourier transform of the non-linear dark matter power spectrum,  $P_{NL}$ . In three dimensions, after assuming space isotropy, this yields

$$\xi_{mm} = \frac{4\pi}{(2\pi)^3} \int P_{NL} \frac{\sin(kr)}{kr} k^2 dk. \quad (3)$$

For the  $\Lambda$ CDM model parameters, the predicted non-linear dark matter model is calculated using the non-linear Halo-fit power spectrum (Smith et al. (2003); Takahashi et al. (2012)).

In terms of the halo mass function,  $\frac{dn(M,z)}{d\ln M}$ , and the linear halo bias,  $b(M, z)$ , that we describe in Section 4 the mean large scale bias is given by

$$b(z) = \frac{1}{\bar{n}} \int d\ln M \frac{dn(M, z)}{d\ln M} \langle N|M \rangle b(M, z) \quad (4)$$

where  $\langle N|M \rangle$  is the mean number of galaxies per halo and  $\bar{n}$  is the mean number density of galaxies given by

$$\bar{n} = \int dM \frac{dn(M, z)}{d\ln M} \langle N|M \rangle. \quad (5)$$

#### 4. Halo mass function and bias in simulations

In this work, first, we study how the halos are biased with respect to the underlying matter distribution using the halo model. Theoretical models for the halo bias have been derived from the mass function (e.g. Mo & White (1996) and Sheth & Tormen (1999)).

We studied the accuracy of the Sheth & Tormen (1999) and Tinker et al. (2010) halo bias model.

We used a halo catalog with the same volume as DES based on the Hubble Volume PO light cone output (Evrard et al. (2002)), extracted from the DES\_v1.02 mock galaxy catalog <sup>2</sup>.

Halos were identified directly on the dark matter lightcone using a spherical over density halo finder.

Since the halo bias is closely related to the description of halo abundance, we first study the theoretical models of the halo abundance. The comoving number density of halos with mass between  $M$  and  $M + dM$  or the unconditional mass function can be written as

$$\frac{dn}{dM} = \frac{\bar{\rho}_m}{M} f(\nu) \frac{d\nu}{dM} \quad (6)$$

where  $f(\nu)$  is the multiplicity function (the fraction of mass in collapsed objects) and  $\bar{\rho}_m$  is the mean comoving mass density. The height of the density peaks is defined

$$\nu \equiv \frac{\delta_c^2}{\sigma^2(M)} \quad (7)$$

where  $\delta_c = 1.686$  is the critical density for spherical collapse and  $\sigma^2(M)$  is the variance of matter density fluctuations on mass scale  $M$ .

Sheth & Tormen (1999) generalized the expression of the Press-Schechter mass function (Press & Schechter (1974)) and calibrated the free parameters using numerical simulations. It can be written as

$$\nu f(\nu) = A(p) \sqrt{\frac{q\nu}{2\pi}} [1 + (q\nu)^{-p}] e^{-\frac{q\nu}{2}} \quad (8)$$

---

<sup>2</sup><http://www.slac.stanford.edu/~mbusha/mocks/catalogs.html>; provided by M. Busha & R. Wechsler

with  $p = 0.3$  and  $q = 0.707$  and  $A(p = 0.3) = 0.322$ .

Tinker et al. (2008) also calibrated fitting functions for the mass function and bias using high resolution simulations. They choose the form

$$\nu f(\nu) = A[1 + (b\nu)^a]\nu^d e^{-\frac{c\nu}{2}} \quad (9)$$

where  $A$ ,  $a$ ,  $b$ ,  $c$  and  $d$  are the free parameters for each overdensity  $\Delta$  value with respect to the mean density of the universe,  $\bar{\rho}_m$ , and were calibrated in simulations at  $z = 0$ . They also provide redshift correction to match mass function to simulations. The halo finder in the DES light cone defines overdense regions with respect to the critical density  $\rho_c(z)$  instead of  $\bar{\rho}_m$ . If we define an overdensity contrast as  $\Delta' = \frac{\Delta}{\Omega_m(z)}$ , we can use this functional form for any value of  $\Delta'$ . The value of the parameters at  $z = 0$  are calculated by spline interpolation as a function of  $\Delta'$  and then we calculate their redshift evolution.

The corresponding large scale halo bias prediction of Sheth & Tormen (1999) is given by

$$b(\nu) = 1 + \frac{q\nu - 1}{\delta_c} + \frac{2p}{\delta_c(1 + (q\nu)^p)}. \quad (10)$$

Later, Tinker et al. (2010) introduces a similar but more flexible fitting function of the form

$$b(\nu) = 1 - A \frac{\nu^a}{\nu^a + \delta_c^a} + B\nu^b + C\nu^C \quad (11)$$

where the parameters also depend on the density contrast  $\Delta$ .

We compare the mass function measured in redshift bins of width  $\Delta z = 0.2$  using the dark matter halo simulation with a DES volume with the Sheth & Tormen (1999) model with  $p$  and  $q$  fiducial values evaluated at the mean redshift. Since there is a high disagreement in all the mass ranges, we fit the parametric model to the halo catalog measurement. Our fitting method is a simple  $\chi^2$  of the difference between the theoretical model and the measured counts in bins (e.g., Jenkins et al. (2001), Manera et al. (2010)

and Manera & Gaztañaga (2011)). We also studied the accuracy of the fitting function for  $\Delta$  overdensities of Tinker et al. (2008). Figure 1 shows the comparison of the systematic error  $\Delta \frac{dn}{dM}$  with the statistical error  $\sigma$  for the two models. In all the redshift bins we found that the deviations,  $\frac{\Delta \frac{dn}{dM}}{\frac{dn}{dM}}$ , increase on the high mass tail for both models where the number of halos is very small. However, these deviations are not significant.

At lower redshift we found the same accuracy for models, however the disagreement between them increases with redshift and we found better accuracy with the Sheth & Tormen (1999) parameters fitted by us. But, of course, one can also fit the Tinker parameters to simulations instead of doing an interpolation and compare again these models. We postpone this work to the future.

We measure the halo linear bias on scales where it is considered to be deterministic and scale independent. We fit the matter correlation function  $\xi_{mm}(r)$  at a given  $z$  to the one measured in the simulations  $\xi_{hh}$  using the Landy & Szalay (1993) estimator. We optimized the Poisson error and made an estimation of the cosmic variance using the jackknife method. Then we compare these measurements with the predictions of the Sheth & Tormen (1999) and the Tinker et al. (2010) bias models as shown in Figure 2. We consider the difference between these two models as a systematic uncertainty of our method. We note also that the bias errors increase with increasing mass and redshift because the number of halos is lower.

## 5. Simulated cluster sample from photometric survey

We created cluster catalogs using the DESv1.02 halo mock catalog light cone mentioned before. The dark matter halos of these simulations are populated with galaxies using a model of HOD: We assign a richness  $N$  to dark matter halos by means of a conditional distribution  $P(N|lnM)$  for a halo of mass  $M$  to contain  $N$  galaxies, where the mass-richness relation is

given by Equation 1.

As discussed in Ikebe et al. (2002), Lima & Hu (2005) and Oguri & Takada (2011), we assumed the scatter in the scaling relation to be log-normally distributed around the mean scaling relations, i.e., Gaussian or normal in  $\ln M$ . Thus, the probability of observing the richness  $N$  given the true underlying mass  $M$  is given by

$$P(N|\ln M, z) = \frac{1}{\sqrt{2\pi\sigma_{\ln M}^2}} \exp\left[-\frac{1}{\sqrt{2\pi\sigma_{\ln M}^2}}(\ln\langle M|N \rangle - \ln M)\right]. \quad (12)$$

In this work we assume the scatter  $\sigma_{\ln M}$  does not vary neither with redshift or mass. Figure 3 shows the HOD distribution,  $P(N|\ln M)$ , with  $\sigma_{\ln M} = 0.2$ . Each point represents the number of galaxies that occupy a particular dark matter halo showing that the observable is noisy. The true underlying mass  $M$  is the halo mass  $M_{200}$ , where  $M_{200}$  is defined as the mass enclosed in a sphere of radius  $R_\Delta$  whose mean density is  $\Delta = 200$  times the threshold density. The halo finder algorithm in the light cone defines spherical regions that are overdense with respect to the critical density  $\rho_c$ . So the  $M_{200}$  mass is given by,

$$M_{200} = \frac{4}{3}\pi\Delta\rho_c R_{200}^3. \quad (13)$$

## 6. Theoretical predictions for the richness bias using the Halo Model

In this section we define a model for the bias for a richness cut  $N > N_{th}$  to compare with the measurements in simulations. This is given by,

$$b(N_{th}, z) = \frac{\sum_{N=N_{th}}^{\infty} b(N, z)n_{meas}(N, z)}{\sum_{N=N_{th}}^{\infty} n_{meas}(N, z)} \quad (14)$$

where  $n_{meas}(N, z)$  is the number of halos per redshift and richness value measured in the simulations, and  $b(N, z)$  is calculated using the halo model of galaxy clustering

$$b(N, z) = \frac{1}{\bar{n}} \int d\ln M \frac{dn(M, z)}{d\ln M} P(\ln M|N) b(M, z) \quad (15)$$

where  $\bar{n}$  is the mean number density of galaxies given by

$$\bar{n} = \int dM \frac{dn(M, z)}{d \ln M} P(\ln M | N) \quad (16)$$

where  $P(\ln M | N)$  is related to the distribution used to create the richness catalog with scatter  $\sigma_{\ln M}$ ,  $P(N | \ln M)$  given by Equation 12, using Bayes' Theorem.

The scatter in the mass-richness relation changes the shape and the amplitude of the mass function above an observable threshold significantly to provide an excess of clusters scattering up (at  $N \leq N_{th}$ ) versus down (at  $N \geq N_{th}$ ). The steepness of the mass function around the observable threshold determines the excess due to upscatters. As the observable threshold reaches the exponential tail of the mass function, the excess of upscatter versus downscatter can become a significant fraction of the total (Lima & Hu 2005) and decrease the bias. The larger is the scatter the more the bias is decreased. Moreover, the impact of the scatter will be significantly greater at high mass and redshift because the steepness of the mass function is larger at high redshift and mass.

## 7. Likelihood analysis. Constraining the scatter

We divide the catalog in redshift bins  $\Delta z$  and make cuts in richness to measure the bias with the two point correlation function. Therefore, we have a set of  $n$  bias measurements,  $b_i^{meas}(N \geq N_{th}, z)$  and their bias errors,  $\sigma_{b_i}^{meas}$ . We assume a model for the bias,  $b^{model}(N_{th}, z)$ , with parameters  $\theta = (\Lambda, \alpha_{M|N}, B_{M|N}, \sigma_{\ln M})$  using Equations 14 and 15. Since our goal is to constrain the scatter, we consider a one dimensional likelihood given by the conditional probability distribution of the data,  $\mathcal{L} = p(b^{meas} | \theta = \sigma_{\ln M})$

$$p(b^{meas}(N_{th}, z); \theta) = \frac{1}{\sqrt{2\pi}\sigma_b^{meas}} \exp \frac{-(b^{meas}(N_{th}, z) - b^{model}(N_{th}, z))^2}{2\sigma_b^{meas}{}^2} \quad (17)$$

where we assume that the measurements are not correlated. Although this is not absolute correct, our plan with data is to divide the catalog in richness bins in we have enough

cluster. In this case the measurements won't be correlated. For  $n$  bias measurements, the likelihood is the product of the probabilities of the individual measurements

$$\mathcal{L} = \prod_{i=1}^n p(b_i^{meas}(N_{th}, z); \theta). \quad (18)$$

Then we normalize the result to the unity. For simplicity, we assume flat priors. We assume known the  $\Lambda$ CDM cosmological parameters of the simulations and we fix the mean mass-richness relation parameters,  $\alpha$  and  $B$ .

### 7.1. Forecast and error estimation using likelihood analysis

Before we study our method in simulations, we make a forecast of the precision that our method can achieve without including the systematics errors coming from the uncertainty in the theoretical bias and mass function model. Instead of the values measured in simulations,  $b_i^{meas}$ , we use the theory predictions for a fiducial model with scatter  $\sigma_{lnM}^{true}$ . We model the bias using using Equations 14 and 15 for 3 samples of richness threshold  $N_{th} \geq 7, 8, 9$  at six redshifts  $z = 0.3, 0.5, 0.7, 0.9, 1.1, 1.3$ . We assign each point an expected experimental error,  $\sigma_{b_i^{measured}}$ , obtained from the fits to the correlation function using the simulations.

Since we perform the likelihood to obtain the best value, we calculate how the richness bias varies with the scatter for a given catalog using Equations 14 and 15. Figure 4 shows the richness bias as a function of the scatter and richness threshold at  $z = 0.3$  using the richness catalog created with  $\sigma_{lnM}^{true} = 0.2$ , where  $n_{measured}(N, z)$  is measured.

Figures 5 and 6 show the recovered values of the scatter,  $\sigma_{lnM}$  and their 68% errors,  $\sigma(\sigma_{lnM})$ . We obtain the same results using Sheth & Tormen (1999) and Tinker et al. (2010) models. Our conclusion is that we may estimate the scatter with a standard deviation or expected error,  $\sigma(\sigma_{lnM})$  (68% C.L), of approximately 0.04, 0.03 and 0.025 for

$\sigma_{lnM}^{true} = 0.1, 0.2, 0.4$  respectively. The precision to measure the scatter is better at larger values because of the slope of the mass function. The larger the scatter the more the bias decreases, in other words, the second derivative of the bias with the scatter is negative,  $\frac{\delta^2 b(N_{th}, z)}{\delta^2 \sigma_{lnM}}$ .

Although the dominant systematic uncertainty in our method comes from the halo mass and bias function, another source of systematics is the mass resolution of the light cone simulations. The minimum halo mass introduces a systematic that affects our richness bias model predictions especially when our observable mass is closer to the minimum. Since we are removing halos from the left side of the lognormal distribution where the bulk of the values lies, the decreasing slope of the bias with the scatter is lower than when we don't remove them. Thus, we will lose precision to recover the scatter as the results show. Moreover, the larger the scatter the larger the disagreement between the two cases and the minimum halo mass systematic is more significant. As an example, when  $\sigma_{lnM}^{true} = 0.4$  the precision decreases, or the expected error increases from  $\sigma(\sigma_{lnM}) = 0.012$  to  $\sigma(\sigma_{lnM}) = 0.025$  (68% *C.L.*).

There are some preliminary results about the mass-richness relation and the scatter using the redMaPPer cluster finder. We want to see if our method will be precise enough for the estimated scatter value in DES. Rykoff et al. (2012) provide a rough calibration of the mass-richness relation using the redMaPPer cluster finder with maxBCG clusters. They give an estimation of the scatter which can be used as the expected value for the DES survey and we can determine the precision of our technique. In addition, early results from the DES SVA data given by Melchior et al. (2015) and Saro et al. (2015) also give an estimation of this quantity. Using these results, we estimate that the intrinsic scatter of the mass-richness relation for the DES survey using redMaPPer is  $\sigma_{lnM} \sim 0.18 - 0.3$  depending of the richness although further work benefiting from a larger region will improve

the constraints. Therefore, using our technique we may constrain the scatter with an expected error,  $\sigma(\sigma_{lnM}) = 0.031 - 0.027$  (68% *C.L.*) using our technique as our predictions show. Moreover, the accuracy will be sufficient for the dark energy parameters not to be significantly biased.

## 7.2. Scatter constrains on simulations

Now that we have studied the bias in halos in the simulations and have made a forecast, we study how well our method can constrain the scatter of the scaling relation using the light cone simulations. Here we add the uncertainty in the theoretical models when we compare with simulations. We perform a likelihood calculation comparing the bias prediction with the measurements for the three catalogs created using dark matter simulations. We assume we know the mean mass-richness relation parameters,  $\alpha$  and  $B$ , and the  $\Lambda$ CDM cosmological parameters of our simulations. Figures 7 and 8 show the scatter constraints and their 68%(C.L) errors for the two theoretical models. As predicted by the forecast, at the largest scatter value,  $\sigma_{lnM}^{true} = 0.4$ , we obtain the best precision and accuracy and the two halo bias prescriptions agree,  $\sigma_{lnM} = 0.399 \pm 0.031$  (68% *C.L.*). However, for lower values there is a discrepancy between them. When the scatter is  $\sigma_{lnM}^{true} = 0.1$  we can not recover the true value in any case while we recover it for  $\sigma_{lnM}^{true} = 0.2$  using the Sheth & Tormen (1999) prescription. In this case the result is  $\sigma_{lnM} = 0.206 \pm 0.035$  (68% *C.L.*). Apart from the redshift uncertainty that we will study soon, we conclude that the theoretical model is the main systematic of this method. Although we can not recover the scatter for the lowest values we still can measure it for the expected value of the DES cluster survey with very good precision.

## 8. Conclusions

In summary, the new method proposed is a promising and powerful method to constrain the scatter using only large optical cluster surveys such as DES, LSST and the Euclid project. This method is complementary to self-calibration and cross-calibration techniques such as the direct method employed by Saro et al. (2015) with a small subset of galaxy clusters. In that study, the mass-richness relation for SZE selected galaxy clusters in the DES Science Verification Area has been preliminarily calibrated. They cross-match the SPT catalog with the redMaPPer and VT cluster catalog. Although this is a very promising technique to use, one of the drawbacks is that it is limited to calibrate SPT-SZE clusters. Our new technique can be used as a cross-check method to compare with those results. In addition, one of the advantages of our method is that it only uses optical clusters and we can measure the scatter in a broader mass range than the SZE clusters. In a near future, the mass-richness relation will be also calibrated in the DES cluster catalog with other mass proxies such as stacked weak lensing shear. At that time we can use this relation as a prior on the mass-richness relation parameters as a function of redshift instead of the one we use from maxBCG clusters.

The main systematic error we have found is the uncertainty in mass function and bias prescription. The difference between the Sheth & Tormen (1999) and Tinker et al. (2010) models is a systematic error. At  $\sigma_{lnM} = 0.4$  both models agree but at lower values the difference increases until it is equal to the statistical precision  $\sigma(\sigma_{lnM})$ . We can not recover the scatter value when the true value is  $\sigma_{lnM} = 0.1$  in any case while we can recover it for  $\sigma_{lnM} = 0.2$  using the Sheth & Tormen (1999) model with our fitted values for p and q. A next step is to perform a calibration of the Tinker parameters in the simulations we used and see if there is still this difference.

Our plan is to implement the new analysis technique in the DES cluster catalogs

to reduce the uncertainty in cosmological parameters coming from an uncertainty in the cosmological parameters. This will be done using the clusters found with the VT cluster finder algorithm and the redMaPPer cluster catalog. Since the DES expected value is around  $0.18 - 0.3$  with redMaPPer catalog, and higher with VT, we conclude that we can measure it precisely enough so that the dark energy parameters won't be significantly biased.

In this work we ignore the effect of the uncertainty of the redshift of the clusters. The effect on the three dimensional correlation function is a smearing of the acoustic peak (Estrada et al. 2009) and a relative damping of power on small scales that reduces the bias. One possible advantage of using clustering of clusters is that the photometric error is lower than it is for galaxies. We postpone a careful study of how this systematic error will affect the bias measurement and the precision of the scatter measurements. This will allow us to use the spatial correlation function (3D) and compare the results with the angular correlation function,  $\omega(\theta)$ .

For future cluster surveys we expect that the statistical errors will be reduced at high mass and redshift because the number of clusters will increase considerably. With this, we forecast higher precision to measure the scatter including the lower values.

We greatly appreciate the support received from the collaborative work Julia Campa undertook with Martin Makler, Mariana Penna and Marc Manera, as we worked together on the theoretical predictions of the halo mass function and bias. We are grateful to Jim Annis, Tom Diehl, Marcelle Soares, Brian Nord, Liz Buckley-Geer, David Finley and Josh Frieman for useful discussions and communications. Thanks again to David Finley for laboriously correcting the grammar and languages mistakes, and made suggestions to what should be explained more. Julia Campa thanks all participants of the Experimental Astrophysics Group meetings at the Fermilab Center for Particle Astrophysics. Thanks

to Eduardo Rozo, Eli Rykoff, Joe Mohr, Christopher Miller, Risa Wechsler and all the participants of the DES cluster working group. Thanks to Michael Busha and Risa Wechsler for providing us the DESv1.02 halo mock catalog light cone survey based on HVS simulations. Julia Campa gratefully acknowledges the funding sources that made this work possible. Much of this work was supported by the Astroparticle Physics Division at Centro de Investigaciones Medioambientales y Energéticas (CIEMAT). This work was partially completed at Fermilab. Julia Campa acknowledges the financial support provided by the Particle Physics Division at Fermilab and the invitations to work at the Fermilab Center for Particle Astrophysics (FCPA).

## REFERENCES

- Abell, G. O. 1958, *ApJS*, 3, 211
- Andreon, S., & Bergé, J. 2012, *A&A*, 547, A117
- Angulo, R. E., Springel, V., White, S. D. M., et al. 2012, *MNRAS*, 426, 2046
- Allen, S. W., Evrard, A. E., & Mantz, A. B. 2011, *ARA&A*, 49, 409
- Bahcall, N. A., & Soneira, R. M. 1983, *ApJ*, 270, 20
- Bahcall, N. A. 1998, *Large Scale Structure: Tracks and Traces*, 137
- Bahcall, N. A., Dong, F., Hao, L., et al. 2003, *ApJ*, 599, 814
- Baugh, C. M. 2013, *PASA*, 30, e030
- Berlind, A. A., & Weinberg, D. H. 2002, *ApJ*, 575, 587
- Bleem, L. E., Stalder, B., Brodwin, M., et al. 2015, *ApJS*, 216, 20
- Bleem, L. E., Stalder, B., de Haan, T., et al. 2015, *ApJS*, 216, 27
- Bocquet, S., Saro, A., Dolag, K., & Mohr, J. J. 2015, *arXiv:1502.07357*
- Böhringer, H., Voges, W., Huchra, J. P., et al. 2000, *ApJS*, 129, 435
- Bonamente, M., Joy, M., LaRoque, S. J., et al. 2008, *ApJ*, 675, 106
- Cataneo, M., Rapetti, D., Schmidt, F., et al. 2015, *Phys. Rev. D*, 92, 044009
- Clifton, T., Ferreira, P. G., Padilla, A., & Skordis, C. 2012, *Phys. Rep.*, 513, 1
- Copeland, E. J., Sami, M., & Tsujikawa, S. 2006, *International Journal of Modern Physics D*, 15, 1753

- Crocce, M., Fosalba, P., Castander, F. J., & Gaztañaga, E. 2010, *MNRAS*, 403, 1353
- Cooray, A., & Sheth, R. 2002, *Phys. Rep.*, 372, 1
- Croft, R. A. C., Matteo, T. D., Khandai, N., et al. 2012, *MNRAS*, 425, 2766
- Einasto, J. 2001, *New A Rev.*, 45, 355
- Eke, V. R., Cole, S., Frenk, C. S., & Patrick Henry, J. 1998, *MNRAS*, 298, 1145
- Estrada, J., Sefusatti, E., & Frieman, J. A. 2009, *ApJ*, 692, 265
- Evrard, A. E., MacFarland, T. J., Couchman, H. M. P., et al. 2002, *ApJ*, 573, 7
- Flaugher, B. 2005, *International Journal of Modern Physics A*, 20, 3121
- Gladders, M. D., & Yee, H. K. C. 2000, *AJ*, 120, 2148
- Haiman, Z., Mohr, J. J., & Holder, G. P. 2001, *ApJ*, 553, 545
- Hao, J., McKay, T. A., Koester, B. P., et al. 2010, *ApJS*, 191, 254
- Ikebe, Y., Reiprich, T. H., Böhringer, H., Tanaka, Y., & Kitayama, T. 2002, *A&A*, 383, 773
- Jenkins, A., Frenk, C. S., White, S. D. M., et al. 2001, *MNRAS*, 321, 372
- Johnston, D. E., Sheldon, E. S., Wechsler, R. H., et al. 2007, *arXiv:0709.1159*
- Koester, B. P., McKay, T. A., Annis, J., et al. 2007, *ApJ*, 660, 239
- Koester, B. P., McKay, T. A., Annis, J., et al. 2007, *ApJ*, 660, 221
- Landy, S. D., & Szalay, A. S. 1993, *ApJ*, 412, 64
- Laureijs, R., Amiaux, J., Arduini, S., et al. 2011, *arXiv:1110.3193*
- Mandelbaum, R., Seljak, U., Hirata, C. M., et al. 2008, *MNRAS*, 386, 781

- Mandelbaum, R., Seljak, U., & Hirata, C. M. 2008, *J. Cosmology Astropart. Phys.*, 8, 006
- Lima, M., & Hu, W. 2007, *Phys. Rev. D*, 76, 123013
- Lima, M., & Hu, W. 2005, *Phys. Rev. D*, 72, 043006
- LSST Dark Energy Science Collaboration 2012, arXiv:1211.0310
- Lukić, Z., Heitmann, K., Habib, S., Bashinsky, S., & Ricker, P. M. 2007, *ApJ*, 671, 1160
- Manera, M., & Gaztañaga, E. 2011, *MNRAS*, 415, 383
- Manera, M., Sheth, R. K., & Scoccimarro, R. 2010, *MNRAS*, 402, 589
- Mo, H. J., & White, S. D. M. 1996, *MNRAS*, 282, 347
- Majumdar, S., & Mohr, J. J. 2004, *ApJ*, 613, 41
- Melchior, P., Suchyta, E., Huff, E., et al. 2015, *MNRAS*, 449, 2219
- Mohr, J. J. 2005, *Observing Dark Energy*, 339, 140
- Neyman, J., & Scott, E. L. 1952, *ApJ*, 116, 144
- Oguri, M., & Takada, M. 2011, *Phys. Rev. D*, 83, 023008
- Pacaud, F., Pierre, M., Adami, C., et al. 2007, *MNRAS*, 382, 1289
- Papovich, C. 2008, *ApJ*, 676, 206
- Planck Collaboration, Ade, P. A. R., Aghanim, N., et al. 2014, *A&A*, 571, A29
- Press, W. H., & Schechter, P. 1974, *ApJ*, 187, 425
- Perlmutter, S., Aldering, G., Goldhaber, G., et al. 1999, *ApJ*, 517, 565
- Pujol, A., & Gaztañaga, E. 2014, *MNRAS*, 442, 1930

- Reed, D., Gardner, J., Quinn, T., et al. 2003, MNRAS, 346, 565
- Reiprich, T. H., & Böhringer, H. 2002, ApJ, 567, 716
- Riess, A. G., Filippenko, A. V., Challis, P., et al. 1998, AJ, 116, 1009
- Rozo, E., Wechsler, R. H., Rykoff, E. S., et al. 2010, ApJ, 708, 645
- Rozo, E., Rykoff, E. S., Evrard, A., et al. 2009, ApJ, 699, 768
- Rozo, E., Rykoff, E., Koester, B., et al. 2011, ApJ, 740, 53
- Rykoff, E. S., Koester, B. P., Rozo, E., et al. 2012, ApJ, 746, 178
- Rykoff, E. S., Rozo, E., Busha, M. T., et al. 2014, ApJ, 785, 104
- Saro, A., Bocquet, S., Rozo, E., et al. 2015, MNRAS, 454, 2305
- Shaw, L. D., Holder, G. P., & Dudley, J. 2010, ApJ, 716, 281
- Sheldon, E. S., Johnston, D. E., Scranton, R., et al. 2009, ApJ, 703, 2217
- Sheth, R. K., & Tormen, G. 1999, MNRAS, 308, 119
- Smith, R. E., Peacock, J. A., Jenkins, A., et al. 2003, MNRAS, 341, 1311
- Soares-Santos, M., de Carvalho, R. R., Annis, J., et al. 2011, ApJ, 727, 45
- Schuecker, P., Böhringer, H., Collins, C. A., & Guzzo, L. 2003, A&A, 398, 867
- Takahashi, R., Sato, M., Nishimichi, T., Taruya, A., & Oguri, M. 2012, ApJ, 761, 152
- The Dark Energy Survey Collaboration 2005, arXiv:astro-ph/0510346
- Tinker, J., Kravtsov, A. V., Klypin, A., et al. 2008, ApJ, 688, 709
- Tinker, J. L., Robertson, B. E., Kravtsov, A. V., et al. 2010, ApJ, 724, 878

- Tinker, J. L., Sheldon, E. S., Wechsler, R. H., et al. 2012, *ApJ*, 745, 16
- Vikhlinin, A., McNamara, B. R., Forman, W., et al. 1998, *ApJ*, 502, 558
- Watson, W. A., Iliev, I. T., D’Aloisio, A., et al. 2013, *MNRAS*, 433, 1230
- Warren, M. S., Abazajian, K., Holz, D. E., & Teodoro, L. 2006, *ApJ*, 646, 881
- Weinberg, D. H., Mortonson, M. J., Eisenstein, D. J., et al. 2013, *Phys. Rep.*, 530, 87
- White, S. D. M., Efstathiou, G., & Frenk, C. S. 1993, *MNRAS*, 262, 1023
- Willis, J. P., Clerc, N., Bremer, M. N., et al. 2013, *MNRAS*, 430, 134
- Yang, X., Mo, H. J., van den Bosch, F. C., & Jing, Y. P. 2005, *MNRAS*, 357, 608
- Zwicky, F., Herzog, E., & Wild, P. 1968, Pasadena: California Institute of Technology (CIT), 1961-1968,

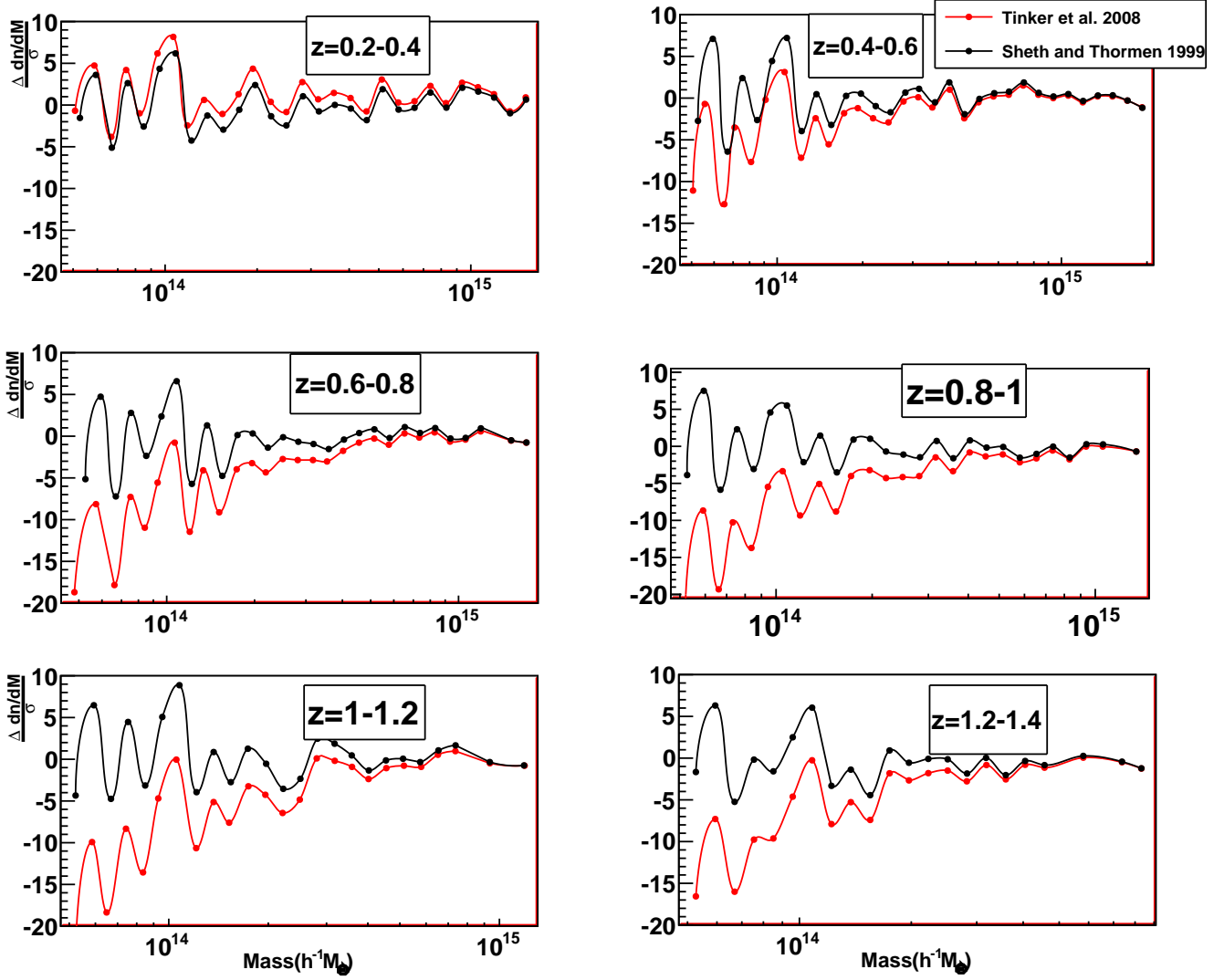


Fig. 1.— Systematic error  $\Delta \frac{dn}{dM}$  compared with the statistical error  $\sigma$  for the six redshift bins from the light cone simulations. Black dots are the values with the Sheth & Tormen (1999) model with the best  $p$  and  $q$  values and red dots are the Tinker et al. (2008) model .

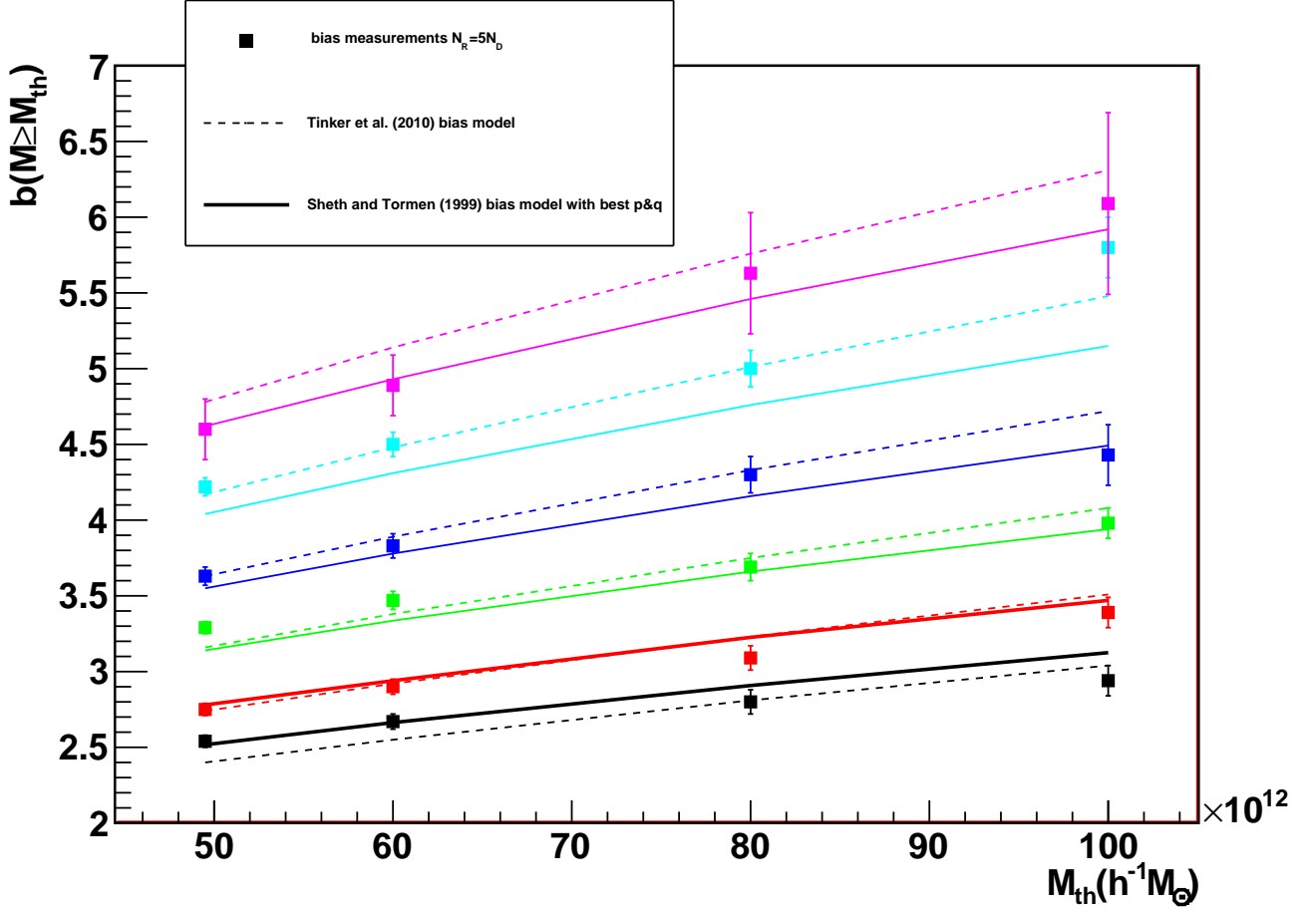


Fig. 2.— Comparison of the halo bias model with the measurements in the light cone for the six redshift bins  $z = 0.2 - 0.4$ ,  $z = 0.4 - 0.6$ ,  $z = 0.6 - 0.8$ ,  $z = 0.8 - 1$ ,  $z = 1 - 1.2$  (black, red, green, blue, cyan and pink dots respectively). The solid curves are the values of the Sheth & Tormen (1999) model with the best  $p$  and  $q$  values and the dashed curves the Tinker et al. (2010) model. The random catalog is 5 times denser than the catalog,  $N_R = 5N_D$  to optimize the Poisson noise.

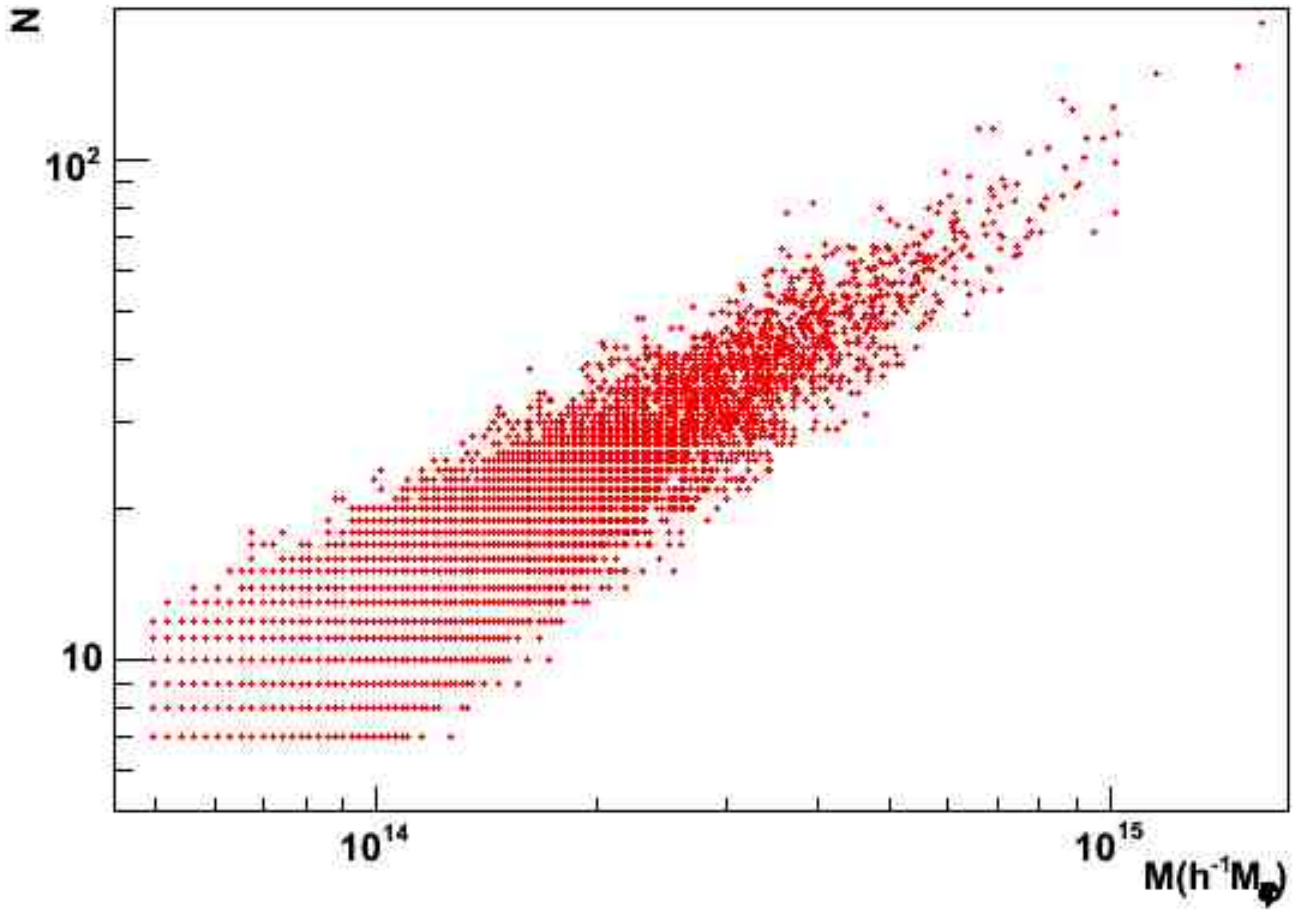


Fig. 3.— HOD distribution,  $P(N|M)$ , when  $\sigma_{\ln M}^{true} = 0.2$

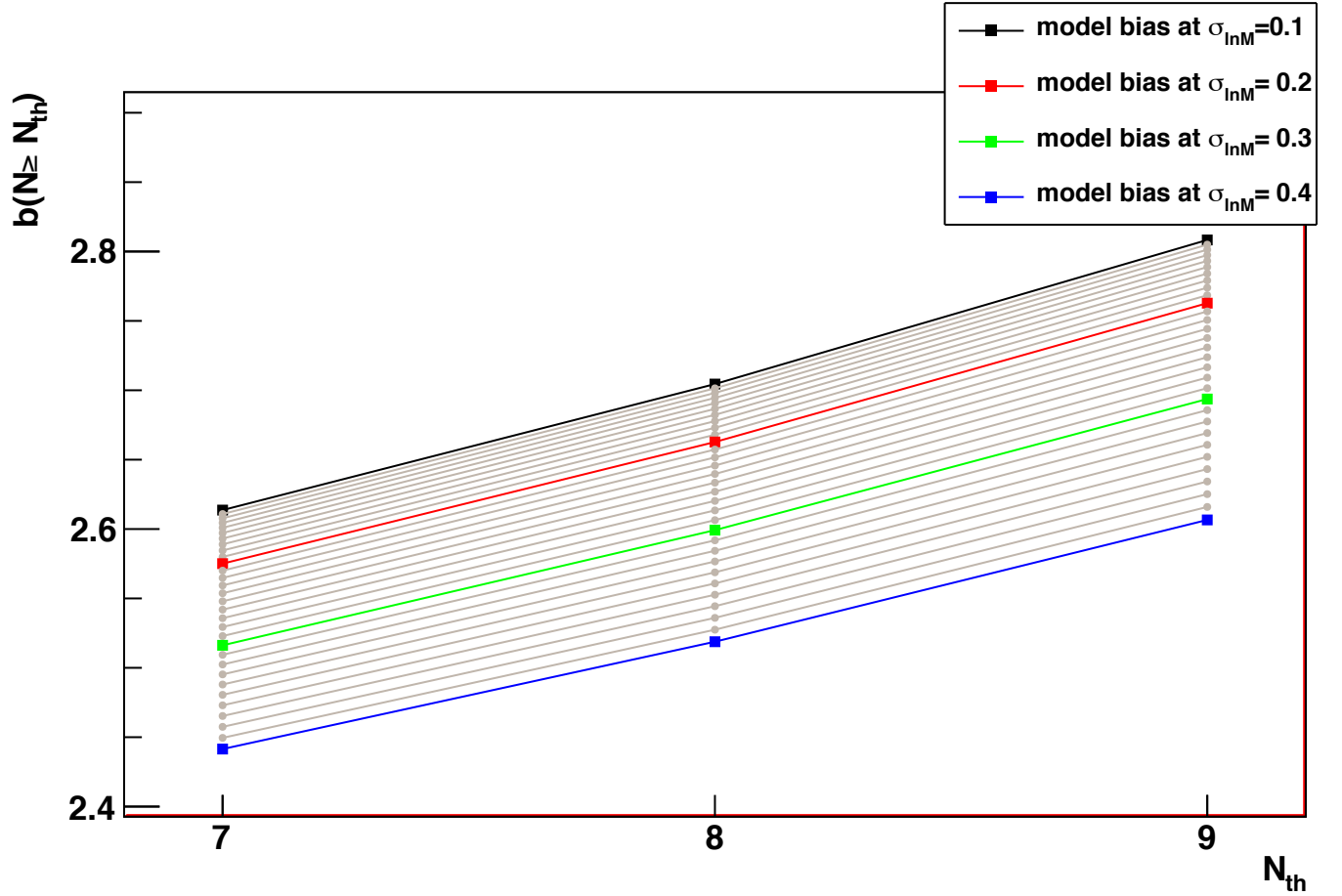


Fig. 4.— Bias model as a function of  $\sigma_{lmM}$  and  $N_{th}$  at  $z = 0.3$  using the catalog created with  $\sigma_{lmM}^{true} = 0.2$

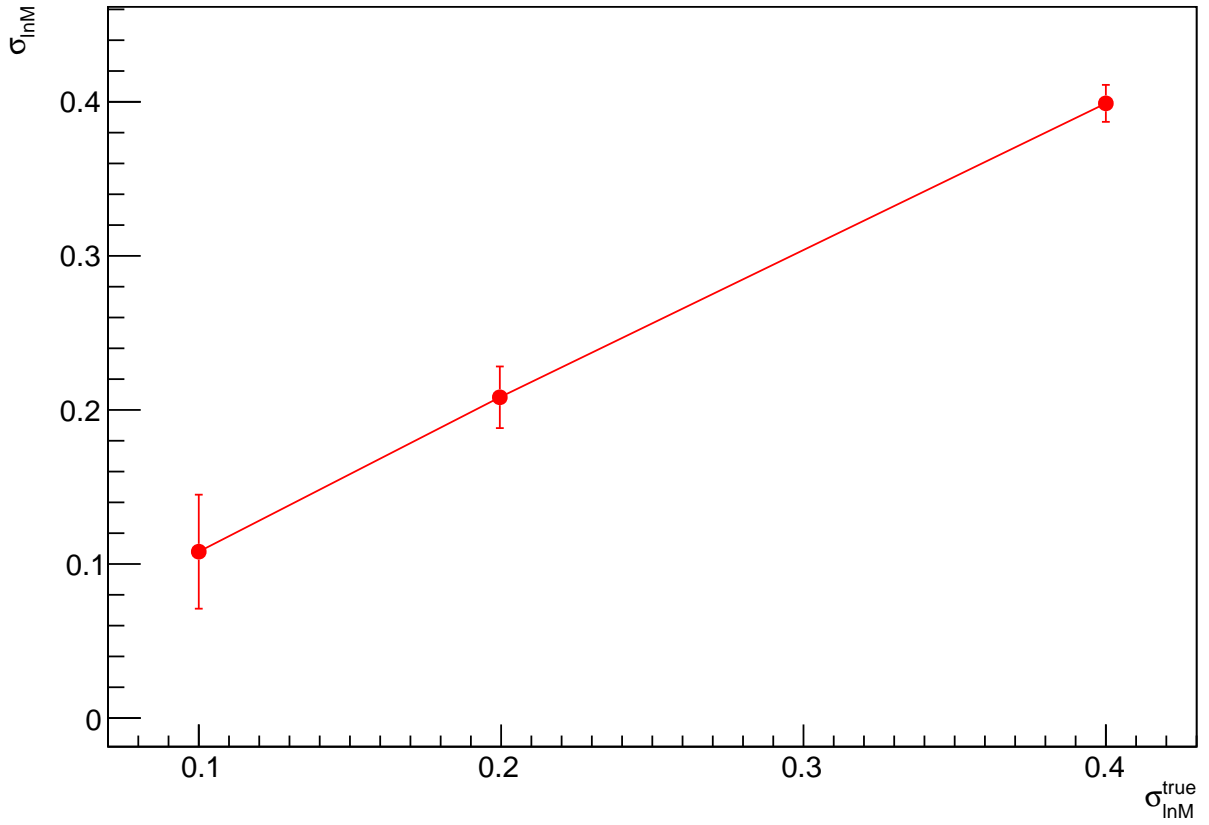


Fig. 5.— Recovered values of the scatter,  $\sigma_{\ln M}$  for different scatter values taken as a fiducial model. The expected errors (68% C.L.)  $\sigma_{\ln M}^{\text{true}}$  are also shown.

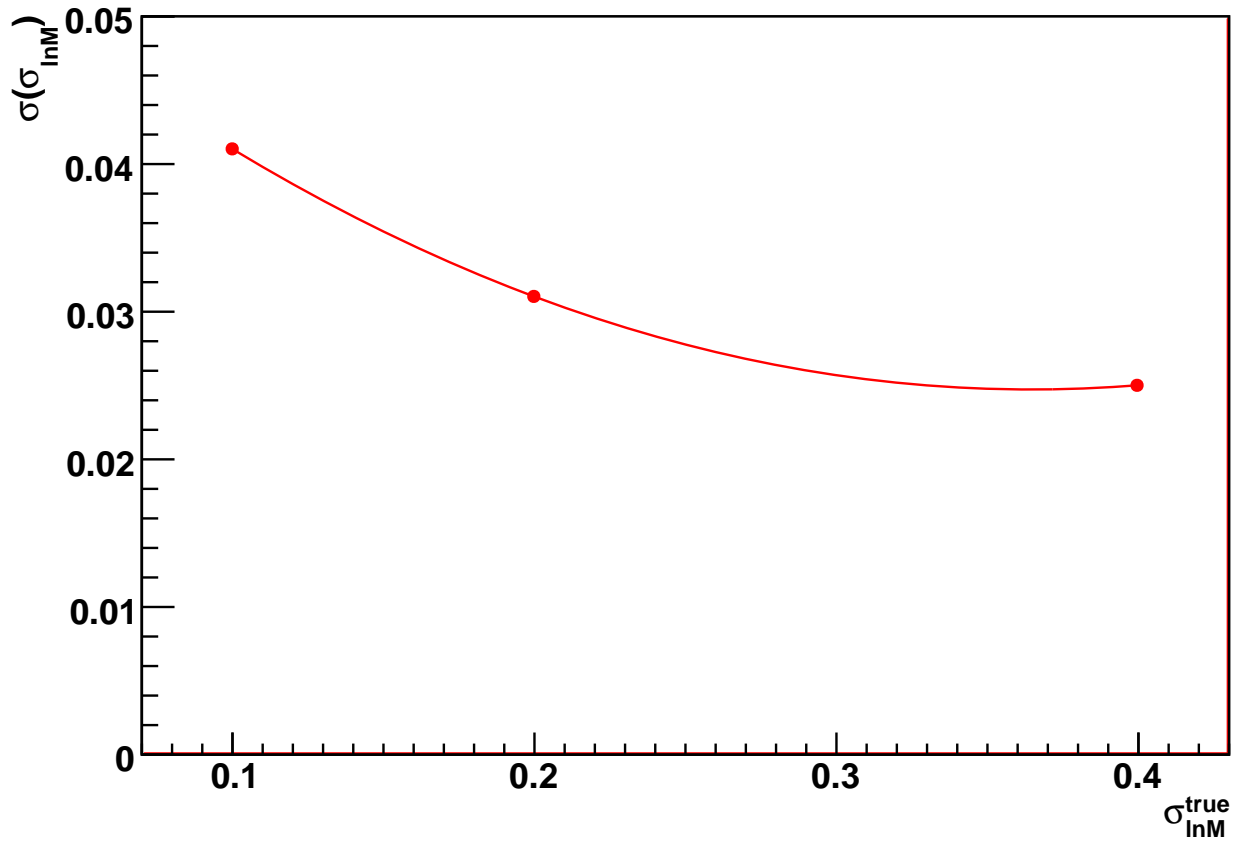


Fig. 6.— Expected errors (68%*C.L.*) for different scatter values taken as fiducial model,  $\sigma_{\ln M}^{\text{true}}$ .

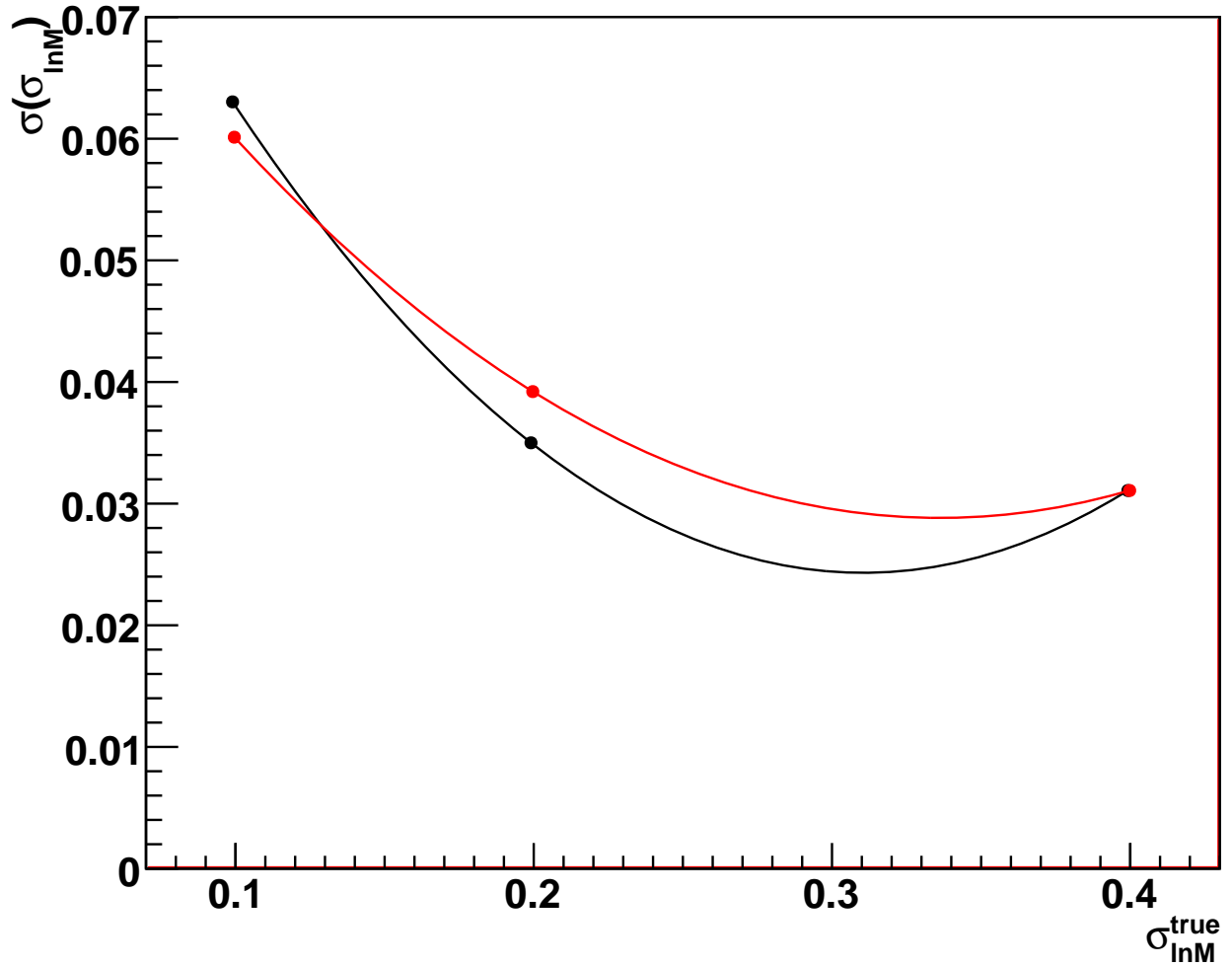


Fig. 7.— Recovered values of the scatter,  $\sigma_{\ln M}$ , for the three catalogs created with  $\sigma_{\ln M}^{\text{true}}$  when we use the Sheth and Thormen (1999) (black dots) and Tinker et al. (2010) (red dots) models. The expected errors (68% *C.L.*) are also shown.

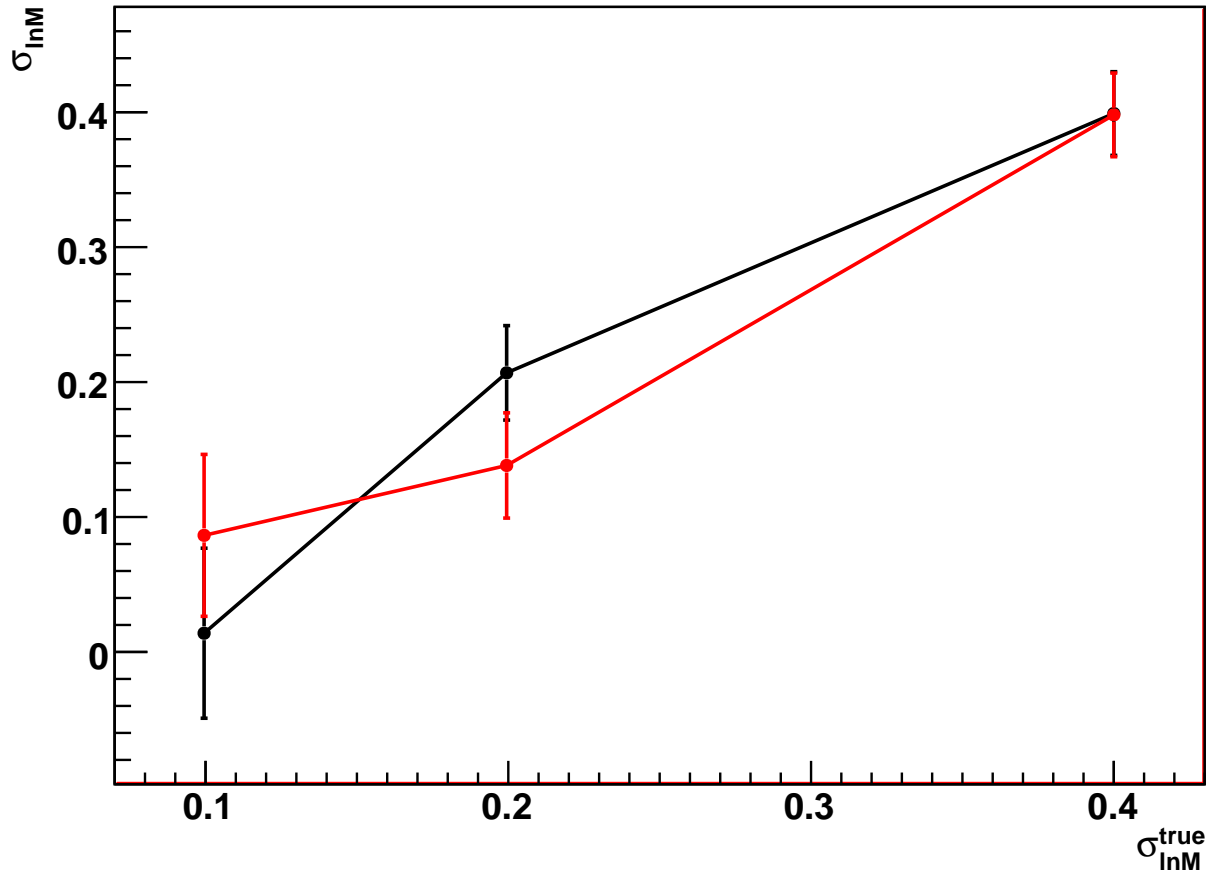


Fig. 8.— Expected errors (68% *C.L.*) for three true scatter values,  $\sigma_{\ln M}^{\text{true}}$  when we use the Sheth and Thormen (1999) (black dots) and Tinker et al. (2010) (red dots) models.